Available online at www.sciencedirect.com

SciVerse ScienceDirect

journal homepage: www.elsevier.com/locate/he

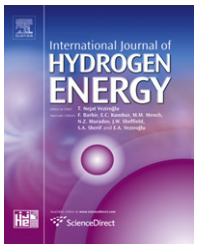

# Oxidative steam reforming of glycerol for hydrogen production: Thermodynamic analysis including different carbon deposits representation and $CO_2$ adsorption

*F. Díaz Alvarado, F. Gracia**

*Departamento de Ingeniería Química y Biotecnología, Facultad de Ciencias Físicas y Matemáticas, Universidad de Chile, Av. Tupper 2069, 2do Piso, Laboratorio de Catálisis y Energía Combustible, 8370451 Santiago, Chile*

ARTICLE INFO

*Article history:*
Received 7 September 2011
Received in revised form
28 December 2011
Accepted 31 January 2012
Available online 3 March 2012

*Keywords:*
Hydrogen
Oxidative steam reforming
Glycerol
Thermodynamics
Carbon deposits
$CO_2$ sorption

ABSTRACT

Glycerol production is associated with growing biodiesel industry, and because of its poor fuel skills it has been signed as a candidate for hydrogen production by Steam Reforming (SR).

In various reforming reaction systems, many different types of Carbon deposits have been reported, but this variety has not been incorporated in thermodynamic studies as previous studies have represented carbon deposits only as Graphite. This work proposes a new representation including Graphite, Carbon Nanotubes, Amorphous, and Polymeric carbon for Glycerol Reforming systems.

The study also includes an analysis of $CO_2$ sorption effects, comparing Hydrotalcites and CaO as sorbents, with their respective variation of sorption capacity with temperature.

All thermodynamic analysis is performed by Gibbs free energy minimization, following an algorithm for discrete nonlinear minimization.

The extended representation of carbon deposits reveals the existence of two regions: below 450 °C the most favorable carbonaceous solid type is graphite; and above, carbon nanotubes.

The use of $CO_2$ sorbents in Glycerol Reforming systems shifts the equilibrium to products, increasing $H_2$ yield. In those systems where Hydrotalcites were included as $CO_2$ sorbent, $H_2$ yield is maximized between 350 °C and 450 °C and S/G ratio above the stoichiometric ratio, while for CaO sorbent and *no sorbent* systems the maximization of $H_2$ yield is given at 600 °C and S/G = 10.

From the thermodynamic analysis, once the O/G ratio has been chosen according to energetic consideration, it is advisable to carry out the Glycerol Reforming reaction with at least a stoichiometric S/G ratio, the addition of enough mass of Hydrotalcites for stoichiometric $CO_2$ sorption and a temperature between 375 °C and 450 °C. Those conditions maximize the $H_2$ yield with no other product gases or carbonaceous solids.



* *Corresponding author*. Tel.: +56 2 9784284.
E-mail addresses: fdiaz.ing@gmail.com (F. Díaz Alvarado), fgracia@ing.uchile.cl (F. Gracia).

0360-3199/$ – see front matter 
doi:10.1016/j.ijhydene.2012.01.158

## 1. Introduction

The Fuel Cell technology and the utilization of Hydrogen as energy carrier have been signed as one of the most promising alternatives for fossil fuels substitution in growing motive and industrial park [1,2]. In addition, Fuel Cells are more energy efficient than internal combustion engines [3].

While oil and natural gas are the main current sources of hydrogen, alcohols have attracted some attention in recent years, specially ethanol [4–7]. Considering alcohols utilization for $H_2$ production by Steam Reforming, the natural progression in alcohol structure and complexity is proposed in Fig. 1. In this sequence, the final goal would be the direct use of vegetal carbohydrates, like glucose, avoiding intermediates for $H_2$ production.

Ethanol, which can be used for renewable production of $H_2$ by Steam Reforming, is being used directly in combustion engines as part of the fuel mixture [8]. Although the direct use of ethanol in motor is not recommended [9], because of the presence of undesirable organic compounds in bioethanol production output, the world demand for this product will grow [5], increasing its price.

On the other hand, glycerol is obtained as a byproduct of biodiesel production in the approximate proportion of 10% of initial oil used. For this reason its global availability is increasing over the years, giving a first incentive for industrial use. Additionally, pure glycerol is a poor fuel and cannot be burned directly in internal combustion engines [10]. Thus, glycerol appears as an alternative for replacement of ethanol in $H_2$ renewable production by Steam Reforming.

The stoichiometry of reaction can be summarized in the following equation [11], by *Oxidative Steam Reforming* (OSR):

$$C_3H_8O_3(l) + (3-2x)H_2O(l) + xO_2(g) \rightarrow 3CO_2(g) + (7-2x)H_2(g)$$
$$\Delta H^0 = 346.5 - 571.7x[kJ/mol] \quad (1)$$

where $x$ is the molar $O_2/C_3H_8O_3$ ratio, abbreviated as O/G ratio; and $H_2O/C_3H_8O_3$ ratio, as S/G ratio (Steam to Glycerol). In the OSR system, endothermic or exothermic conditions can be modulated by adjusting the O/G ratio, which also determine the stoichiometric S/G ratio. $\Delta H^0$ for global reaction moves from 346.5 [kJ/mol], at O/G = 0, to −82.3 [kJ/mol], at O/G = 0.75. In relation to overall thermodynamics, the energy system is neutral when $x = 0.61$ in the above equation. The operation at this point is called *Autothermal Reforming* (ATR). If no $O_2$ is added the reaction system is called *Steam Reforming* (SR) of Glycerol.

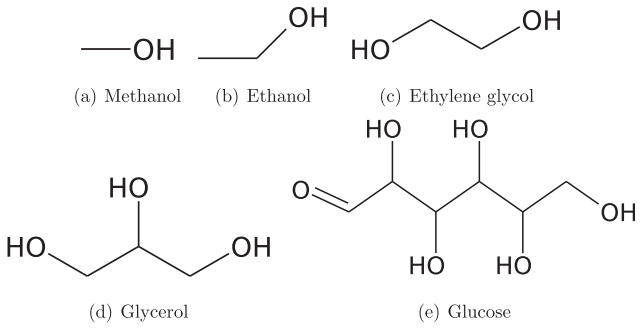


**Fig. 1 – Progression for alcohol structure and complexity for $H_2$ production by Steam Reforming.**

The carbonic solid formation has to be avoided because of catalyst deactivation, so its representation becomes important. There are publications on Thermodynamics of SR and OSR systems of Glycerol that do consider the formation of solid carbon deposits, but these are represented exclusively as Graphite [12–14], while others include only gaseous species [15,16].

But Graphite is not the only possible structure for the carbonaceous deposits, since the presence of Amorphous carbon deposits has been reported in Reforming systems [17–19]. Also Carbon Nanotubes have been detected over Reforming catalyst [20–22], which production is favored at high temperatures [23]. The structure of carbonaceous deposits formed in a catalytic process depends on reaction pathway, catalyst characteristics and reaction conditions. According to these specifications, in a catalytic process is possible to obtain various types of carbonaceous deposits, that differ in morphology and reactivity [19,24,25]. A study developed over Ni catalyst has shown five types of carbon deposits [23].

The use of Graphite thermodynamic properties for the whole carbonaceous deposits representation can be, then, considered incomplete. The representation of those deposits and the gases evolved in reaction system can be adequately constructed based on their thermodynamic properties [26–28].

Through thermodynamic analysis the effect of $CO_2$ sorbents in the Reforming system can also be analyzed to quantify how $CO_2$ sorption would shift the equilibrium to products. Up to now, the thermodynamic equilibrium has been calculated with the inclusion of CaO [29], but the use of Hydrotalcites could be attractive because its maximum sorption capacity is given at lower temperatures [30,31].

This work analyzes the thermodynamic equilibrium composition of Oxidative Steam Reforming of Glycerol, considering an extended representation of carbon deposits, including Graphite, Nanotubes, Amorphous and Polymeric carbon. The analysis also includes the use of Hydrotalcites as sorbent of $CO_2$.

## 2. Methodology

For predicting the thermodynamic equilibrium composition by minimization of the Gibbs free energy function, the expression given in Equation (2) has to be minimized.

$$G = \sum_{i=1}^{NC^g} n_i^g \left(\mu_i^{g,0} + RT\ln\left(\hat{f}_i\right)\right) + \sum_{i=1}^{NC^s} n_i^s \mu_i^{s,0} \quad (2)$$

In equation (2), $NC^g$ and $NC^s$ are the number of components in gas and solid phase, respectively; $n_i^g$, the number of moles of component $i$ in gas phase; $n_i^s$, the number of moles of component $i$ in solid phase; $R$, the gas constant in [J/mol K]; $T$, the temperature in [K]; $\hat{f}_i$ is the fugacity of component $i$ in a multi-component solution (dimensionless); and $\mu_i^0 = \mu_i^0(T)$ is

the chemical potential of species i at standard pressure, focusing on Enthalpy information [32].

$$\left(\frac{\partial \underline{H}_i}{\partial T}\right)_P = c_{p_i} \tag{3}$$

$$\frac{\partial}{\partial T}\left(\frac{\underline{G}_i}{RT}\right)_P = -\frac{\underline{H}_i}{RT^2} \tag{4}$$

$$\underline{G}_i = \mu_i \tag{5}$$

The chemical potential can be calculated from equations (3)–(5), where $\underline{G}_i$ is the partial molar Gibbs Free Energy; $\underline{H}_i$, the partial molar Enthalpy; and $c_{p_i}$, the heat capacity at constant pressure of component i [33–35].

$$Z - 1 = \frac{P_r}{T_r}\left(B^0 + \omega B^1\right) \tag{6}$$

The fugacity ($\hat{f}_i$, where $\hat{}$ denotes the estimation in a multi-component solution) was calculated under the assumption of real gases representation by a Virial Equation of State (VEOS) (equation (6)) [36] and excluding solid from the calculation of the gas molar fraction. In this equation, $P_r$ is the reduced pressure; $T_r$, the reduced temperature; and $\omega$, the acentric factor.

$$y_i = \frac{n_i^g}{n_{gases}} \tag{7}$$

$$\hat{f}_i = y_i \cdot P \cdot \hat{\phi}_i \tag{8}$$

In equation (7), $n_{gases}$ defines the total number of moles in gas phase; and, in equation (8), P is the dimensionless pressure ($P_{eval}/P_{std}$).

$$\hat{\phi}_i = \phi_i \tag{9}$$

Equation (9) is the Lewis/Randall rule for an ideal solution model, and allows the calculation of fugacity coefficient of component i in the multi-component solution ($\hat{\phi}_i$) as the one for isolated species ($\phi_i$). It can be calculated from equation (10).

$$\phi_i = \exp\left(\frac{\frac{y_i P}{P_{c_i}}}{\frac{T}{T_{c_i}}}\left(B_i^0 + \omega B_i^1\right)\right) \tag{10}$$

Equation (10) was derived from VEOS, where $P_{c_i}$ is the dimensionless critical pressure of component i (Critical pressure/$P_{std}$), while $T_{c_i}$ and $\omega_i$ are the critical temperature and the acentric factor of component i, respectively. Terms $B_i^0$ and $B_i^1$ were calculated from Pitzer correlation [36], available in equations (11) and (12).

$$B_i^0 = 0.083 - \frac{0.422}{\left(\frac{T}{T_{c_i}}\right)^{1.6}} \tag{11}$$

$$B_i^1 = 0.139 - \frac{0.172}{\left(\frac{T}{T_{c_i}}\right)^{4.2}} \tag{12}$$

All the data for $P_{c_i}$, $T_{c_i}$, $\omega_i$, $\Delta G_{f_i}^0$, $\Delta H_{f_i}^0$ and $C_{1_i}$ to $C_{5_i}$ (constants for polynomial expression of $c_{p_i}$), required for the calculation of Gibbs free energy of gaseous species, were taken from international databases [26,27]. For graphite, nanotubes and amorphous carbon, $\Delta G_{f_i}^0$, $\Delta H_{f_i}^0$ and $c_{p_i}$ were calculated as in our previous work [37] from databases [38–40]. Polymeric carbon was represented as polyethylene, considered the simplest polymer, with less stringent formation conditions than polypropylene, for example. This allows to assume a more favorable Gibbs free energy of formation than other types of polymer. If the equilibrium composition contains polyethylene, then it would be possible to suggest the representation of other types of more complex polymers; if not, is not possible to have other types of polymer at thermodynamic equilibrium, sustained on its relative Gibbs free energies. The properties for polyethylene were taken from polymer thermodynamic data [41,42], fixing $\Delta G_{f_{Polyethylene}}^0$ and $\Delta H_{f_{Polyethylene}}^0$ as −2187.83 [J/mol] and 7117.56 [J/mol], respectively.

For Hydrotalcites (Mg50) representation, Ficicilar and Dogu [31] suggested the general formula $Mg_{2y}Al_2(OH)_{4y}$, where y is 1.25 for Mg50, reaching a $MgO:Al_2O_3$ ratio of 1. The change in Hydrotalcites when $CO_2$ is adsorbed can be represented by $MgO_{(s)} + CO_{2_{(g)}} \rightleftarrows MgCO_{3_{(s)}}$. So $\Delta G_{f_i}^0$, $\Delta H_{f_i}^0$ and $c_{p_i}$ for these solids were taken from databases [28].

The $CO_2$ sorption capacity for Hydrotalcites was included as an upper bound for the yield of sorbent-$CO_2$ complex. The considered sorption capacity depends on temperature, as shown in Fig. 2.

The mass of Hydrotalcites included in the different calculations is such that the adsorption of the entire stoichiometric production of $CO_2$ at maximum sorption capacity of Hydrotalcites (430 °C) is possible. The process of $CO_2$ adsorption on Hydrotalcites was represented up to 450 °C, where Hydrotalcites-like structures are destroyed [43].

The effect of $CO_2$ sorption on thermodynamic equilibrium composition was also analyzed for a more common CaO sorbent. CaO sorption capacity also varies with temperature [44,45], and the considered variation is available in Fig. 2.

Similarly to $CO_2$ sorption on Hydrotalcites, the adsorption on CaO was represented as formation of $CaCO_3$, and the mass of CaO was such that allows the adsorption of the entire production of $CO_2$ at the maximum sorption capacity of CaO (700 °C). CaO and $CaCO_3$ thermodynamic properties were taken from databases [28].

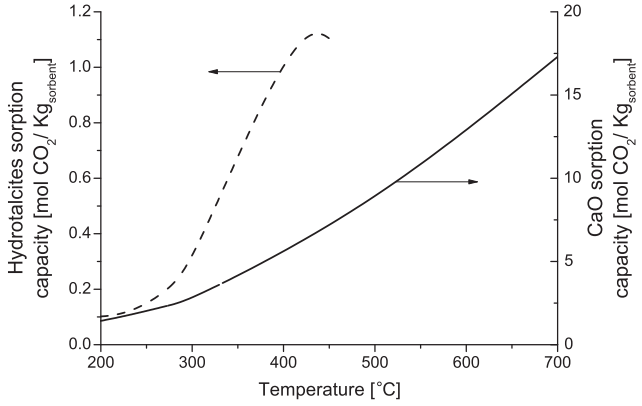


**Fig. 2 – Sorption capacity for Hydrotalcites [30,31] and CaO [44,45] considered in this study.**

Therefore, 3 alternatives for $CO_2$ sorption were considered for the Glycerol Reforming systems: *no sorbent*, *Hydrotalcites sorbent* and *CaO sorbent*.

All calculations were performed in GNU Octave [46] with QtOctave editor [47] following an algorithm for discrete nonlinear minimization detailed elsewhere [37]. A set of 35 molecules were considered as possible species:

- *Gases*: glycerol, oxygen, water, carbon dioxide, hydrogen, carbon monoxide, methane, ethane, ethylene, acetylene, acetaldehyde, acetic acid, acetone, ethyl acetate, diethyl ether, ethylene glycol, *n*-propanol, iso-propanol, *n*-butanol, isopropyl methyl ether, propane, propene, propadiene, allyl alcohol, propionic acid, acrylic acid, methyl ethyl ether, *n*-propion aldehyde and acrolein.
- *Solids*: graphite, carbon nanotubes, amorphous carbon, polyethylene, magnesium oxide and magnesium carbonate (last two for the representation of $CO_2$ sorption with Hydrotalcites), calcium oxide and calcium carbonate (last two for the representation of $CO_2$ sorption with CaO).

The atomic balance and non-negative constraints were included as in a previous work [37], and all calculations were performed at atmospheric pressure.

## 3. Results

### 3.1. *Extended carbon deposits representation*

The composition of gases and solids at thermodynamic equilibrium depends on the system conditions (Temperature, S/G ratio and O/G ratio). When all carbon deposits are represented as Graphite, the formation of carbonaceous solids appears to be favored below 700 °C and S/G ratio under 4.0 (Fig. 3a), when no Oxygen is present. When O/G ratio grows, all carbon formation regions are included in those margins. The extended carbon deposits representation reveals the existence of two regions: below 450 °C the most favorable carbonaceous solid type is graphite (Fig. 3b); and above, nanotubes (Fig. 3c). This boundary moves to lower temperatures (425 °C), when S/G ratio grows over 3.0 (Fig. 4a). With the extended representation, the equilibrium composition for carbon deposits shows higher values than the composition calculated with only graphite. Is possible to note this difference in Fig. 4a above 450 °C, in carbon nanotubes region, for S/G ratios below 3.0. So, the yield for carbonaceous solids at thermodynamic equilibrium is higher than calculated up to now for Steam Reforming of Glycerol above 450 °C. Consequently, the $H_2$ yield is usually overestimated when only graphite is considered. This is confirmed in Fig. 4b, where the difference in carbon deposits yield leads to lower Hydrogen, Carbon monoxide and Carbon dioxide yields between 450 °C and 600 °C, and higher Methane yields in the same region.

With the data used in his work, there is no formation of Amorphous or Polymeric carbon (represented as polyethylene) at thermodynamic equilibrium. Thus, it is likely that amorphous carbon formation reported on Glycerol Reforming catalysts can be related with the kinetics of carbon deposition far from equilibrium.

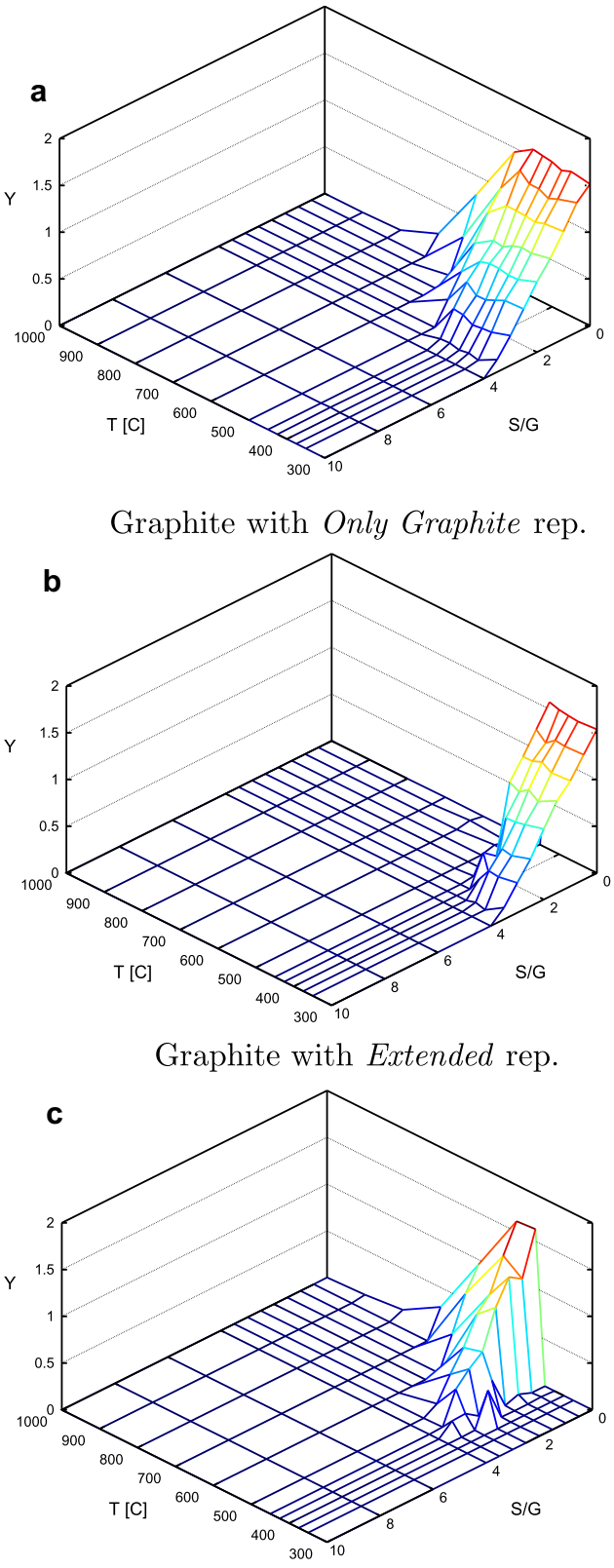


**Fig. 3 – Carbonaceous deposits yield [mol/mol$_{Glycerol}$] with *Only Graphite* and *Extended* representation with O/G = 0 and no sorbent.**

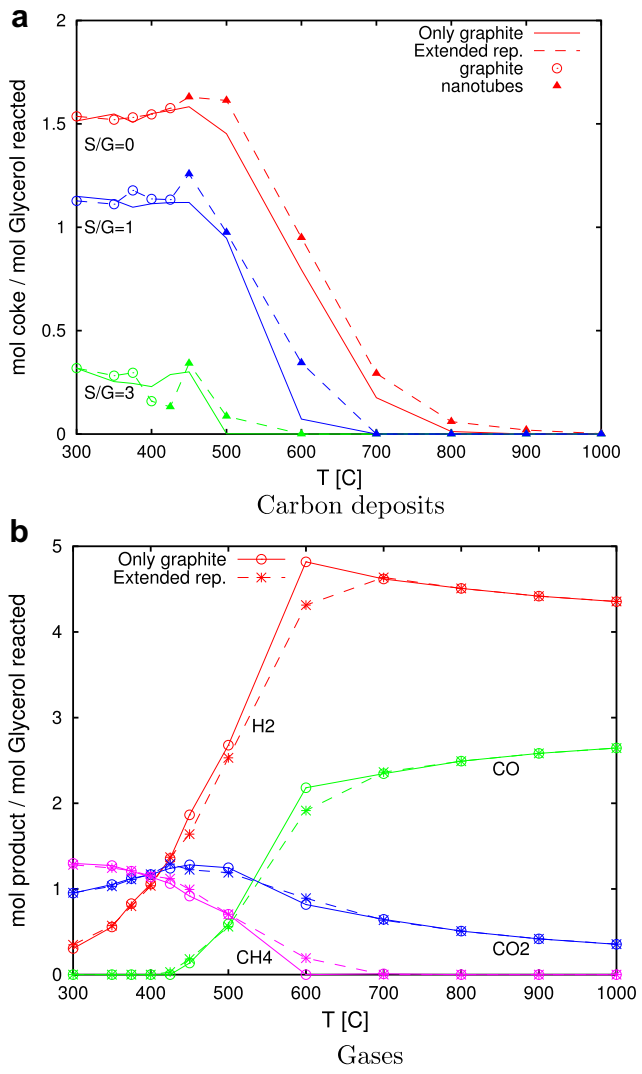


**Fig. 4 – Carbonaceous deposits and gaseous yield [mol/mol$_{Glycerol}$] with *Only Graphite* and *Extended* representation with O/G = 0, S/G = 2.0 and no sorbent.**

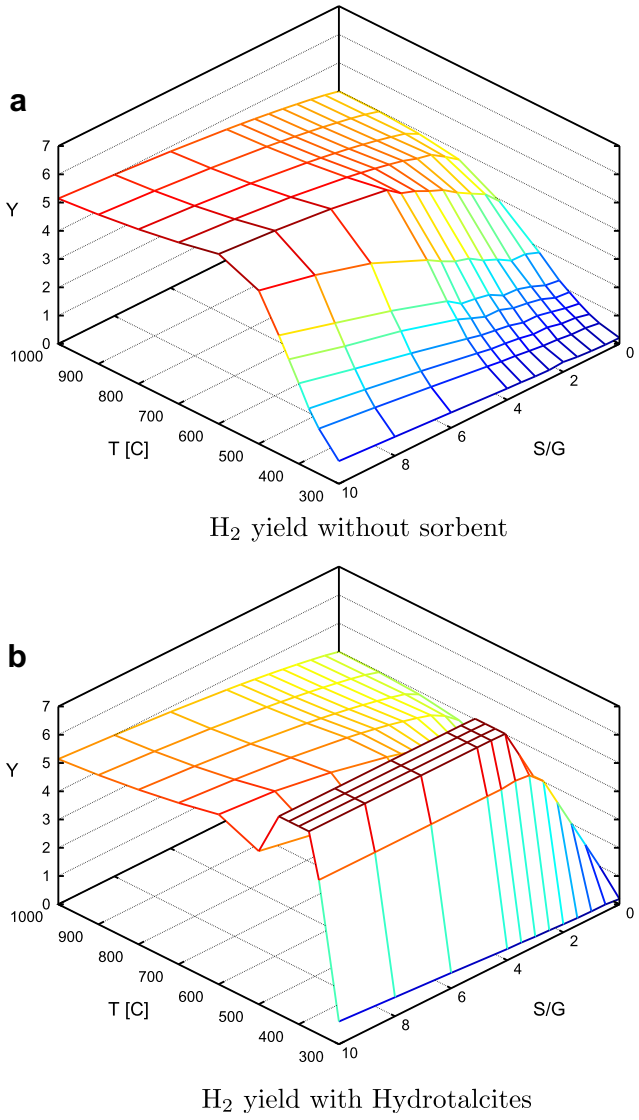


**Fig. 5 – Hydrogen yield [mol$_{H_2}$/mol$_{Glycerol}$] without $CO_2$ sorption and with Hydrotalcites, at O/G = 0.**

### 3.2. *Hydrotalcites effect*

The removal of a product from a reaction system shifts the equilibrium conversion to the products side.

Hydrotalcites can be used for $CO_2$ sorption, but its sorption capacity varies with temperature [30,31]. If this behavior is incorporated in thermodynamic equilibrium calculations, then is expected to obtain higher yields for $H_2$, the non-sorbed product, where $CO_2$ sorption is maximum.

A zero $CO_2$ yield shifts the $H_2$ equilibrium yield from 6.0 [mol$_{H_2}$/mol$_{Glycerol}$], for the *no sorbent* case, to 7.0 [mol$_{H_2}$/mol$_{Glycerol}$], as can be seen in Fig. 5. Those two distinct maximums are achieved at different conditions: when $CO_2$ is adsorbed with Hydrotalcites, the maximum yield of $H_2$ is achieved between 375 °C and 450 °C and above a S/G ratio of 3.0 (stoichiometric); and without sorbents, at 600 °C and a S/G ratio of 10.0.

Then, the maximum yield of $H_2$ is 7.0 [mol$_{H_2}$/mol$_{Glycerol}$], and it is achieved between 375 °C and 450 °C when Hydrotalcites are present, within the region of maximum $CO_2$ sorption (350 °C–450 °C) (Fig. 5b). It is interesting to note that maximum $H_2$ yield is obtained within a temperature range, and not exclusively at 430 °C, where the sorption capacity of Hydrotalcites is maximum. This behavior is caused by the variation of $CO_2$ equilibrium yield with temperature. In the case that no sorbent is present, the $CO_2$ production is continuously increasing until the maximum yield reached at 500 °C (Fig. 6a). Whereas, if sorption on Hydrotalcites is considered, the total sorption capacity of the mass of sorbent is enough to remove completely the $CO_2$ from the gas mixture between 350 °C and 450 °C (and not only at 430 °C), as can be seen in Fig. 6b. In must be noted that below 350 °C, $CO_2$ sorption is not thermodynamically favorable, as can be demonstrated comparing the respective regions in Fig. 6.

The effect of $CO_2$ sorption with Hydrotalcites in carbon deposits equilibrium composition is shown in Fig. 7. As in *no sorbent* case, Graphite formation is favorable below S/G ratio of 4.0, when O/G ratio is 0, and all other formation boundaries

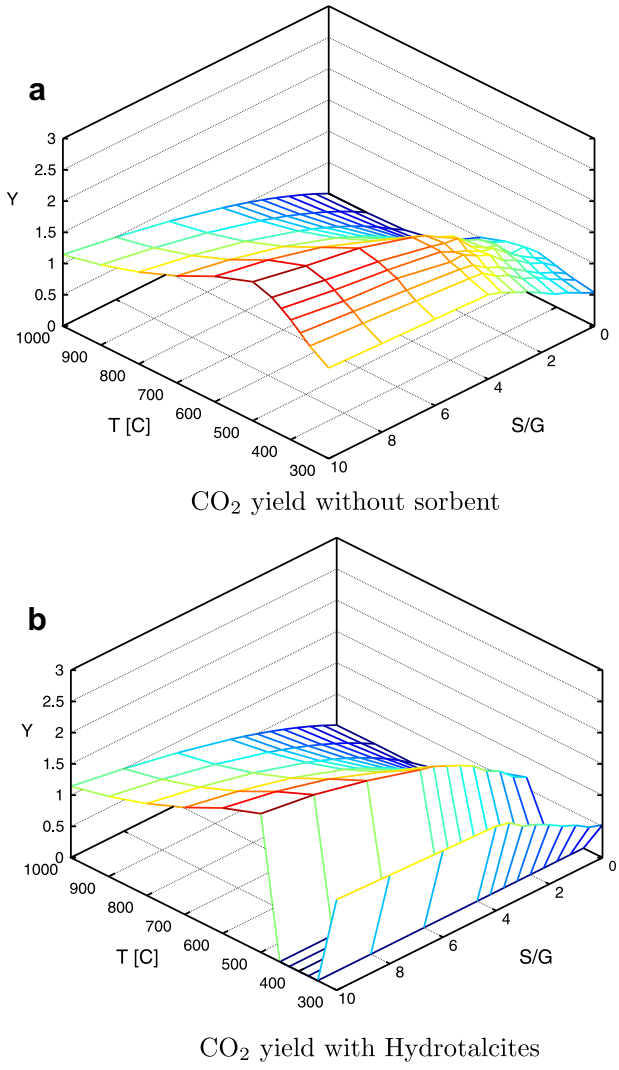


**Fig. 6 – Carbon dioxide yield [mol/mol$_{Glycerol}$] without $CO_2$ sorption and with Hydrotalcites, at O/G = 0.**

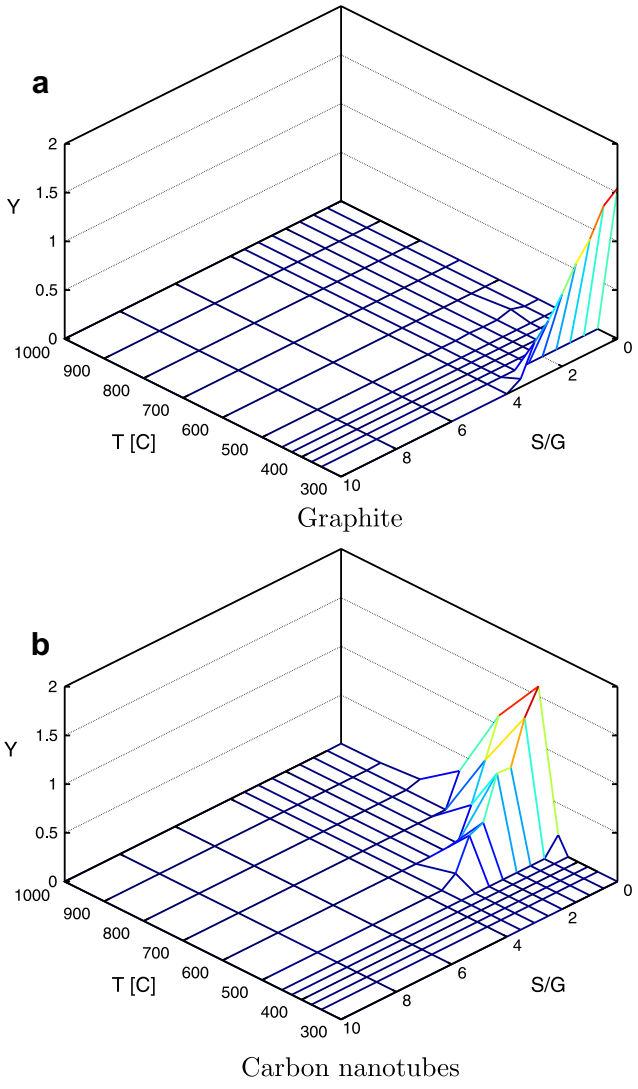


**Fig. 7 – Carbonaceous deposits yield [mol/mol$_{Glycerol}$] with *Extended* representation, O/G = 0 and $CO_2$ sorption with Hydrotalcites.**

(for other O/G ratios) are included in this first interval. But the upper bound for Graphite formation region related with temperature is different when $CO_2$ sorption changes: in *no sorbent* case, Graphite formation is favorable up to 450 °C (Fig. 3b), but when $CO_2$ sorption with Hydrotalcites is incorporated, Graphite formation is favored only up to 350 °C (Fig. 7a). This effect matches with $CO_2$ sorption profile just analyzed. Then $CO_2$ and Graphite are both unfavorable between 350 °C and 450 °C when Hydrotalcites-like sorbent is incorporated, region where the formation of sorbent + $CO_2$ complex becomes favorable.

The effect of $CO_2$ sorption with Hydrotalcites on carbon nanotubes profile includes only the 450 °C isothermal cut. At this temperature, carbon nanotubes formation is favorable when no $CO_2$ sorbent is present (Fig. 3c), but unfavorable when Hydrotalcites are included in the system (Fig. 7b).

The thermodynamic influence of Hydrotalcites on Glycerol Reforming systems can be compared with CaO. As can be seen in Fig. 8, the maximum $H_2$ yield for CaO sorbent systems is 6.85 [mol$_{H_2}$/mol$_{Glycerol}$], and is achieved at 600 °C and

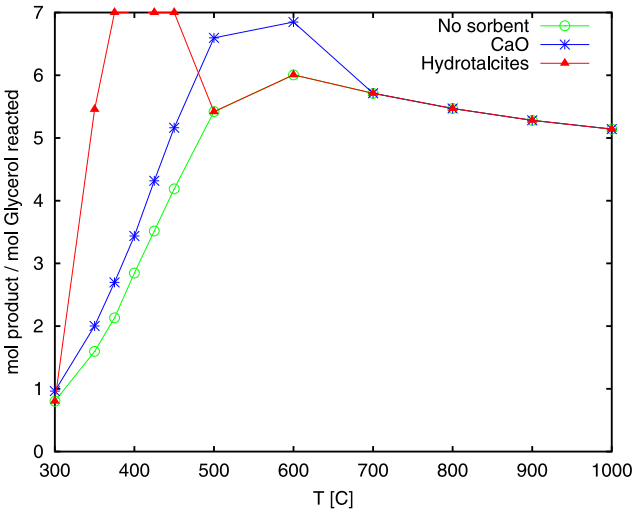


**Fig. 8 – Hydrogen yield [mol$_{H_2}$/mol$_{Glycerol}$] with different sorbents, O/G = 0 and S/G = 10.0.**

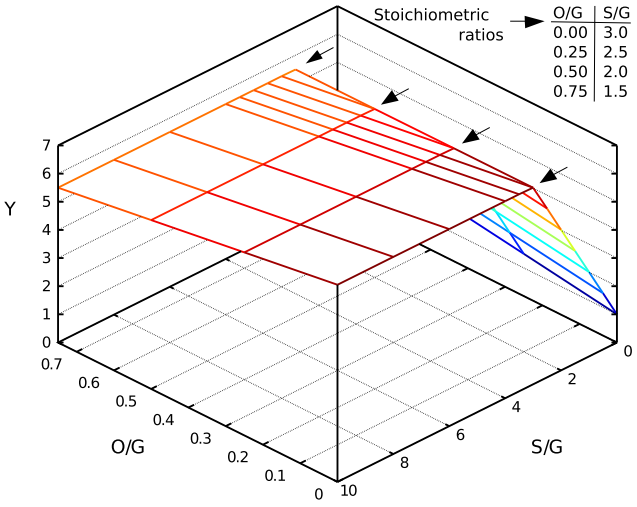


**Fig. 9 – Hydrogen yield [$mol_{H_2}/mol_{Glycerol}$] with different S/G and O/G ratios at T = 375 °C and Hydrotalcites as $CO_2$ sorbent. Stoichiometric S/G and O/G ratios for the analysis of oxygen effect are tabulated and marked with arrows.**

S/G = 10.00, when O/G ratio is set as 0. In conclusion, the equilibrium yield for $H_2$ can be maximized by the use of Hydrotalcites as $CO_2$ sorbent. This maximum has a higher value than that for $H_2$ yield in CaO sorbent system, and is obtained at lower temperature: 350 °C–450 °C for Hydrotalcites, instead of 600 °C for CaO sorbent system (see Fig. 8). In both cases the $H_2$ equilibrium yield is higher than that in the *no sorbent* system, in agreement with the expected shift in global reaction.

### 3.3. *Oxygen effect*

Oxygen is used in Reforming processes for avoiding carbon deposition and improving energetic sustainability of the whole process, sacrificing to some extent the $H_2$ yield.

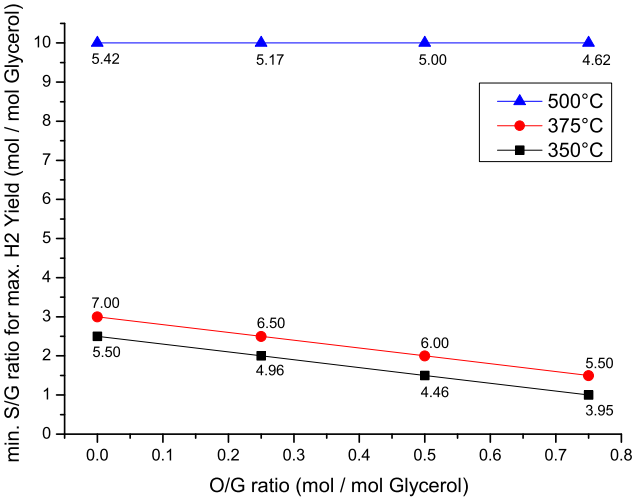


**Fig. 10 – Minimum S/G ratio for maximum $H_2$ yield [$mol_{H_2}/mol_{Glycerol}$] O/G ratios and temperatures and Hydrotalcites as $CO_2$ sorbent. Maximum values for $H_2$ yield are informed as labels.**

The use of Oxygen also modifies the equilibrium composition. Fig. 9 shows the Hydrogen yield with $CO_2$ sorption with Hydrotalcites at 375 °C, for various O/G and S/G ratios. Taking into account the stoichiometric relation between Glycerol, Oxygen and Water exposed in Eq. (1), Fig. 9 shows that the growth of S/G ratio from stoichiometric does not affect the Hydrogen yield, when Hydrotalcites are present. This behavior is different from that of *no sorbent* systems (Fig. 5a), where the S/G ratio over stoichiometry does modify the Hydrogen yield. Then, to study the effect of O/G ratio on the equilibrium of Glycerol Reforming when Hydrotalcites are present, S/G ratio should be stoichiometric at least. Thus, in the following analysis, S/G ratio has been set as stoichiometric for each O/G ratio, following Eq. (1). This means that as O/G ratio increases (x value in Eq. (1)) the S/G ratio decreases according to the stoichiometric coefficient 3 – 2x. This setting

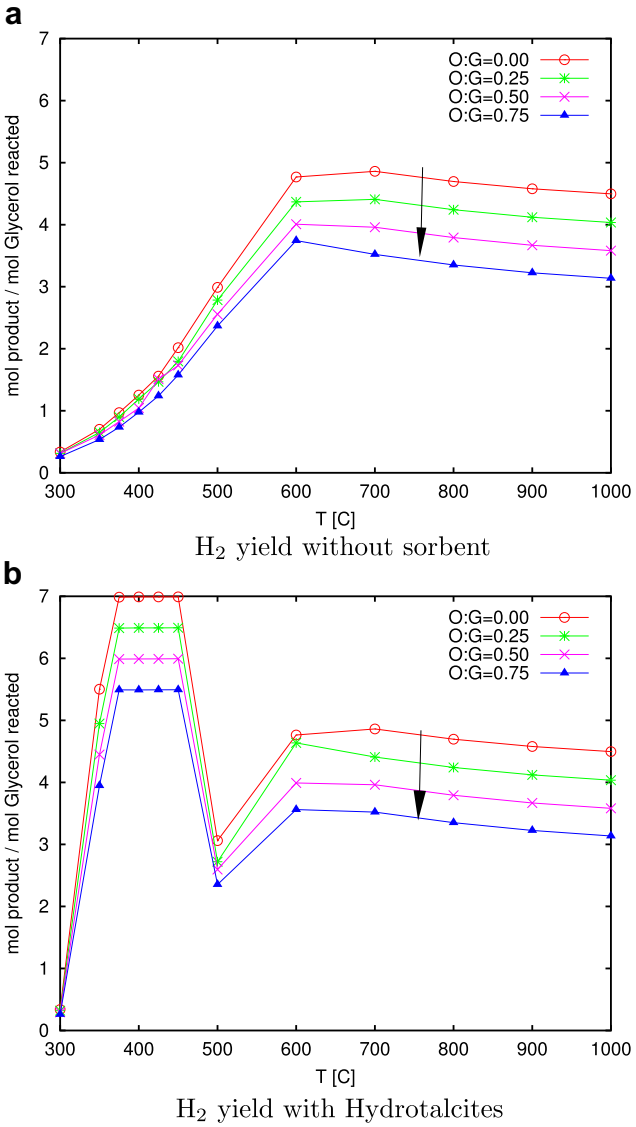


**Fig. 11 – Hydrogen yield [$mol_{H_2}/mol_{Glycerol}$] with *Extended* representation of carbonaceous solids and different sorbents and O/G ratios. S/G ratio was set as stoichiometric for each O/G ratio, following Eq. (1). The direction of O/G ratio growth is informed with an arrow.**

allows to study the effect of O/G ratio without dealing with water lack nor excess, optimizing the water content. The chosen S/G and O/G ratios are informed in Fig. 9, where stoichiometric S/G and O/G ratios for analysis are tabulated and marked with arrows.

Fig. 10 is a representation of minimum S/G ratio required for maximum $H_2$ yield as a function of O/G, at various temperatures. The maximum value of Hydrogen yield obtained at equilibrium is informed as a label next to each point. The temperatures chosen in this figure are related with the activity of Hydrotalcites: at 350 °C Hydrotalcites are active, but at equilibrium there is no $CO_2$ capture (Fig. 6b), because it is thermodynamically not favorable; at 375 °C Hydrotalcites are active, the sorption of $CO_2$ is favorable and the sorption capacity of Hydrotalcites is enough for capturing all the $CO_2$ from equilibrium (as mentioned before, this complete $CO_2$ capture from equilibrium remains constant up to 450 °C); and at 500 °C Hydrotalcites are not active, due to the destruction of its structure, so $CO_2$ sorption profile returns to *non sorbent* conditions. Fig. 10 shows that above 500 °C, where Hydrotalcites structure is destroyed, the increase of the S/G ratio over the stoichiometric value can improve the yield of $H_2$ up to a value of 5.42 $[mol_{H_2}/mol_{Glycerol}]$, but is not possible to reach the maximum theoretical yield, 7.0 $[mol_{H_2}/mol_{Glycerol}]$. This value is only available for no oxygen systems (O/G = 0), when Hydrotalcites are used as $CO_2$ sorbents, within the temperature range between 375 °C and 450 °C.

As expected, Hydrogen yield shows a decrease when O/G ratio grows, as shown in Fig. 11, linked with a shift to exothermic conditions as $\Delta H^0$ for global reaction moves from 346.5 [kJ/mol], at O/G = 0, to −82.3 [kJ/mol], at O/G = 0.75. Is important to note that a growth in O/G ratio is linked with a decrease in S/G ratio, given the stoichiometric proportion herein maintained. It is, then, reasonable to obtain less $H_2$ yield with higher O/G ratio, because there are less water molecules in the system (and therefore initially less Hydrogen atoms in the system).

In the absence of $CO_2$ sorbents the maximum $H_2$ yield is 4.86 $[mol_{H_2}/mol_{Glycerol}]$ for O/G = 0. Upon an increase of oxygen concentration this yield decreases even further, reaching a maximum $H_2$ yield of 3.74 $[mol_{H_2}/mol_{Glycerol}]$ for O/G = 0.75 at 600 °C and stoichiometric S/G ratio. Even though, in presence of the $CO_2$ sorbent, an increase of the O/G ratio also affects the $H_2$ yield, by using Hydrotalcites the $H_2$ yield can be maintained above 5.5 $[mol_{H_2}/mol_{Glycerol}]$ even for high oxygen concentration (O/G = 0.75).

Specifically, Hydrotalcites addition could compensate the loss in $H_2$ yield associated with the growth of the O/G ratio (Fig. 11), keeping its equilibrium value above 5.5 $[mol_{H_2}/mol_{Glycerol}]$ when the O/G ratio is below 0.75 and the temperature is between 350 °C and 450 °C, as seen in Fig. 11b. $H_2$ maximum yield obtained at O/G = 0.75 when Hydrotalcites are present (Fig. 11b) is higher than the maximum yield for $H_2$ at O/G = 0 without $CO_2$ sorbent (Fig. 11a).

Finally, the effect of the O/G ratio on the carbon containing species profile can be seen in Fig. 12. An increase of the O/G ratio, with a stoichiometric water concentration, leads to a raise in carbon deposits equilibrium yield. This behavior is

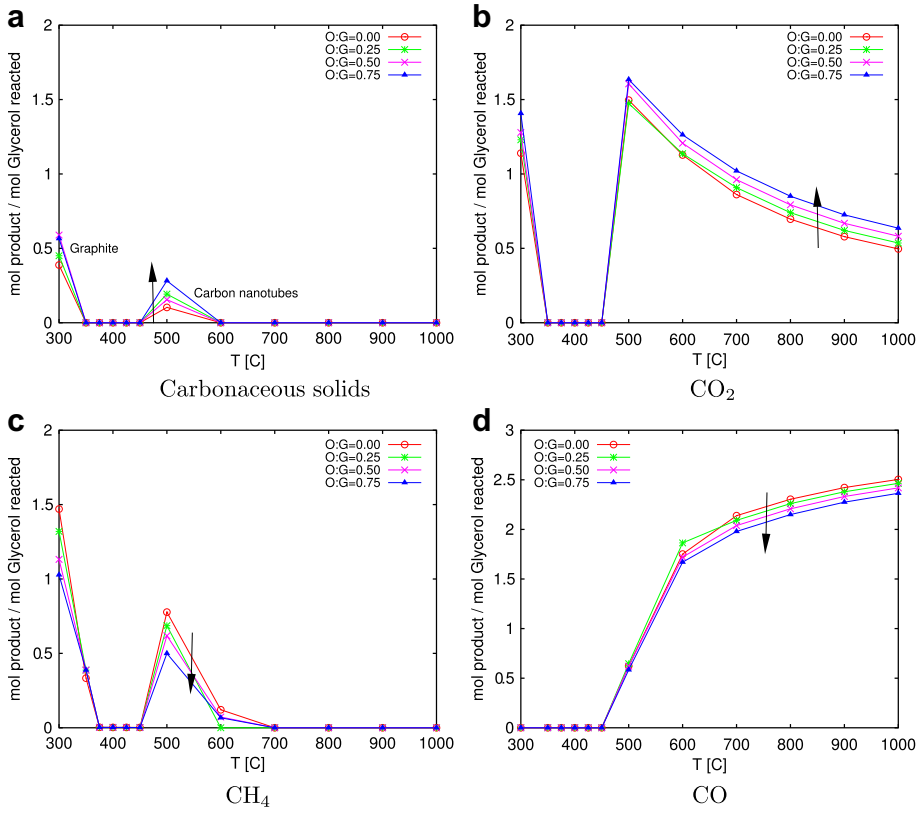


**Fig. 12 – Carbonaceous products yield $[mol/mol_{Glycerol}]$ with *Extended* representation of carbonaceous solids, Hydrotalcites as $CO_2$ sorbent and different O/G ratios. S/G ratio was set as stoichiometric for each O/G ratio, following Eq. (1). The direction of O/G ratio growth is informed with an arrow.**

related with the formation or disappearance of the other C-containing gases (Fig. 12): CO and $CH_4$ yields decrease with O/G ratio growth, while $CO_2$ increases its equilibrium yield. Thus, an O/G ratio growth, linked with a stoichiometric S/G ratio decrease, shifts the global equilibrium, making more favorable the formation of highly oxidized products ($CO_2$). These changes also affect the formation of hydrogenated products ($H_2$ and $CH_4$).

It must be noted that all these effects can be avoided between 350 °C and 450 °C if Hydrotalcites are used as $CO_2$ sorbents. Specifically, between 375 °C and 450 °C, there is no other product gases at thermodynamic equilibrium than $H_2$, and there is no carbon deposits, as can be seen in Figs. 11b and 12.

## 4. Conclusion

Traditional representation of carbon deposits for thermodynamic study of Glycerol Reforming system includes only graphite. This is an incomplete representation, since more types of carbonaceous solids have been reported. The extended representation of carbon deposits reveals the existence of two regions: below 450 °C the most favorable carbonaceous solid type is graphite; and above, carbon nanotubes.

There is no Amorphous or Polymeric carbon (represented as polyethylene) at equilibrium, no matter what temperature, S/G or O/G ratio is chosen.

The use of $CO_2$ sorbents in SR and OSR of Glycerol shifts the equilibrium to products, increasing $H_2$ yield. In those systems where Hydrotalcites were included as $CO_2$ sorbent, $H_2$ yield is maximized between 350 °C and 450 °C, while for CaO sorbent the maximization of $H_2$ yield is given at 600 °C. The maximum for Hydrotalcites system is also higher, reaching 7 $[mol_{H_2}/mol_{Glycerol}]$ for O/G = 0 and S/G ratio above 3.0, against 6.85 $[mol_{H_2}/mol_{Glycerol}]$ for CaO system and 6.0 $[mol_{H_2}/mol_{Glycerol}]$ for *no sorbent* system, both at same O/G ratio and S/G = 10.0.

For all O/G ratios, when Hydrotalcites were used for $CO_2$ sorption the results show higher $H_2$ yields than CaO and *no sorbent* systems, and those values were available at lower S/G ratios and lower temperatures.

The addition of oxygen favors the energetic sustainability of the whole process, but affects $H_2$ formation. An increase of the O/G ratio, with a stoichiometric S/G ratio, shifts the thermodynamic equilibrium to $CO_2$ formation, making less favorable the formation of $H_2$, $CH_4$ and CO, and more favorable the formation of carbon deposits, as a consequence of minor C-containing gases yield. This trend can be avoided between 375 °C and 450 °C by using Hydrotalcites as $CO_2$ sorbent, as no $CO_2$, CO, $CH_4$ nor carbon deposits are observed at thermodynamic equilibrium, and $H_2$ yield is maximized. From the thermodynamic analysis, once the O/G ratio has been chosen according to energetic considerations, it is advisable to carry out the Glycerol Reforming reaction with at least a stoichiometric S/G ratio, the addition of enough mass of Hydrotalcites for total $CO_2$ sorption and a temperature between 375 °C and 450 °C. Those conditions maximize the $H_2$ yield with no other product gases or carbonaceous solids.

## Acknowledgments

The funding from Fondecyt project N°1090232, and CONICYT Doctoral Fellowship (F. Díaz Alvarado) are gratefully acknowledged.

## REFERENCES

[1] Marbán G, Valdés-Solís T. Towards the hydrogen economy? International Journal of Hydrogen Energy 2007;32(12):1625–37. URL: http://www.sciencedirect.com/science/article/B6V3F-4MYMNTF-5/2/e5d74164f600f57645c3dcf7085ae0a5.

[2] Marbán G, Valdés-Solís T. Corrigendum to "Towards the hydrogen economy" [Int. J. Hyd. Energy 32(12) (2007) 1625–1637]. International Journal of Hydrogen Energy 2008;33(2). URL: http://www.sciencedirect.com/science/article/B6V3F-4R8PN5V-5/2/476276eabe68b1d7c3e5222717fefe1d. p. 927.

[3] Örücü E, Karakaya M, AvcI AK, Önsan ZI. Investigation of ethanol conversion for hydrogen fuel cells using computer simulations. Journal of Chemical Technology & Biotechnology 2005;80(10):1103–10. URL: http://dx.doi.org/10.1002/jctb.1288.

[4] Fatsikostas A, Kondarides D, Verykios X. Production of hydrogen for fuel cells by reformation of biomass-derived ethanol. Catalysis Today 2002;75(1–4):145–55. URL: http://www.sciencedirect.com/science/article/B6TFG-458P9FB-J/2/bb6d13d3ac55aae5c13fe3fd298a6dae.

[5] Vaidya PD, Rodrigues AE. Insight into steam reforming of ethanol to produce hydrogen for fuel cells. Chemical Engineering Journal 2006;117(1):39–49. URL: http://www.sciencedirect.com/science/article/B6TFJ-4J2M5NP-6/2/c2820dc93d98c5fe86831a800e5adea2.

[6] Haryanto A, Fernando S, Murali N, Adhikari S. Current status of hydrogen production techniques by steam reforming of ethanol: a review. Energy & Fuels 2005;19(5):2098–106. URL: http://pubs3.acs.org/acs/journals/doilookup?in_doi=10.1021/ef0500538.

[7] Önsan ZI. Catalytic processes for clean hydrogen production from hydrocarbons. Turkish Journal of Chemistry 2007;31:531–50. URL: http://journals.tubitak.gov.tr/chem/issues/kim-07-31-5/kim-31-5-14-0706-22.pdf.

[8] Goldemberg J. The Brazilian biofuels industry. Biotechnology for Biofuels 2008;1:1–7. doi:10.1186/1754-6834-1-6. URL: http://dx.doi.org/10.1186/1754-6834-1-6.

[9] Cavallaro S. Ethanol steam reforming on $Rh/Al_2O_3$ catalysts. Energy & Fuels 2000;14(6):1195–9. URL: http://pubs3.acs.org/acs/journals/doilookup?in_doi=10.1021/ef0000779.

[10] Scharmer K, Vermeersch G, Andronico G. Engine fuel from rapeseed, Tech. Rep.; 2006.

[11] Joensen F, Rostrup-Nielsen JR. Conversion of hydrocarbons and alcohols for fuel cells. Journal of Power Sources 2002;105(2):195–201. URL: http://www.sciencedirect.com/science/article/B6TH1-449V2XG-2/2/951318c7dfb9357241eab2548a600c72.

[12] Wang X, Wang N, Li M, Li S, Wang S, Ma X. Hydrogen production by glycerol steam reforming with in situ hydrogen separation: a thermodynamic investigation. International Journal of Hydrogen Energy 2010;35(19):10252–6. URL: http://www.sciencedirect.com/science/article/B6V3F-50VGHF6-6/2/d644bd43357eb1e4cb4e82ccd76ff114.

[13] Dieuzeide ML, Amadeo N. Thermodynamic analysis of glycerol steam reforming. Chemical Engineering and

Technology 2010;33(1):89–96. URL: http://dx.doi.org/10.1002/ceat.200900260.
[14] Li Y, Wang W, Chen B, Cao Y. Thermodynamic analysis of hydrogen production via glycerol steam reforming with $CO_2$ adsorption. International Journal of Hydrogen Energy 2010; 35(15):7768–77. URL: http://www.sciencedirect.com/science/article/B6V3F-509Y43Y-7/2/53777adc15101d151309b073c2af613c.
[15] Luo N, Zhao X, Cao F, Xiao T, Fang D. Thermodynamic study on hydrogen generation from different glycerol reforming processes. Energy & Fuels 2007;21(6):3505–12. URL: http://dx.doi.org/10.1021/ef070066g.
[16] Authayanun S, Arpornwichanop A, Paengjuntuek W, Assabumrungrat S. Thermodynamic study of hydrogen production from crude glycerol autothermal reforming for fuel cell applications. International Journal of Hydrogen Energy 2010;35(13):6617–23. URL: http://www.sciencedirect.com/science/article/B6V3F-5037MCH-3/2/767b8f47708bd3371239185ac53a463a.
[17] Wang H, Liu Y, Wang L, Qin Y. Study on the carbon deposition in steam reforming of ethanol over $CO/CeO_2$ catalyst. Chemical Engineering Journal 2008;145(1):25–31. URL: http://www.sciencedirect.com/science/article/B6TFJ-4S0JN5X-1/2/80cc84dc4020aa45955b89dfeb772731.
[18] Song H, Ozkan US. Ethanol steam reforming over co-based catalysts: role of oxygen mobility. Journal of Catalysis 2009; 261(1):66–74. URL: http://www.sciencedirect.com/science/article/B6WHJ-4V28T1N-1/2/81898912dea8b41ce6a94aff68b56d84.
[19] Osswald S, Havel M, Gogotsi Y. Monitoring oxidation of multiwalled carbon nanotubes by Raman spectroscopy. Journal of Raman Spectroscopy 2007;38(6):728–36. URL: http://dx.doi.org/10.1002/jrs.1686.
[20] Frusteri F, Freni S, Chiodo V, Donato S, Bonura G, Cavallaro S. Steam and auto-thermal reforming of bio-ethanol over MgO and $CeO_2$ Ni supported catalysts. International Journal of Hydrogen Energy 2006;31(15):2193–9. URL: http://www.sciencedirect.com/science/article/B6V3F-4JN2NPM-2/2/ec78869247add8f219ba3c504d121c7b.
[21] Cavallaro S, Chiodo V, Freni S, Mondello N, Frusteri F. Performance of $Rh/Al_2O_3$ catalyst in the steam reforming of ethanol: $H_2$ production for MCFC. Applied Catalysis A: General 2003;249(1):119–28. URL: http://www.sciencedirect.com/science/article/B6TF5-48GVV1J-1/2/b983e7c94e1ddf3ef69aef52c3bf6919.
[22] Virginie M, Araque M, Roger A-C, Vargas JC, Kiennemann A. Comparative study of $H_2$ production by ethanol steam reforming on $Ce_2Zr_{1.5}Co_{0.5}O_8$-[delta] and $Ce_2Zr_{1.5}Co_{0.47}Rh_{0.07}O_8$-[delta]: evidence of the Rh role on the deactivation process. Catalysis Today 2008;138(1–2):21–7. URL: http://www.sciencedirect.com/science/article/B6TFG-4ST4CF1-2/2/f27fa8b0cc07d743221f5ff80b6a2342.
[23] Bartholomew CH. Carbon deposition in steam reforming and methanation. Catalysis Reviews, Science and Engineering 1982;24:67–112.
[24] Bartholomew CH. Mechanisms of catalyst deactivation. Applied Catalysis A: General 2001;212(1–2):17–60. URL: http://www.sciencedirect.com/science/article/B6TF5-430G359-3/2/33397707733299bfcbd32b45060d723c.
[25] Ginsburg JM, Piña J, El Solh T, de Lasa HI. Coke formation over a nickel catalyst under methane dry reforming conditions: thermodynamic and kinetic models. Industrial & Engineering Chemistry Research 2005;44(14): 4846–54. URL: http://pubs.acs.org/doi/abs/10.1021/ie0496333.
[26] NIST. NIST chemistry WebBook. The National Institute of Standards and Technology, U.S. Secretary of Commerce. URL: http://webbook.nist.gov/; 2005.
[27] CHERIC. Korea thermophysical properties data bank. Chemical Engineering Research Information Center. URL: http://www.cheric.org/research/kdb/; 2009.
[28] Chase M. NIST-JANAF thermochemical tables. New York: American Chemical Society; 1998.
[29] Lima da Silva I, Müller L. Hydrogen production by sorption enhanced steam reforming of oxygenated hydrocarbons (ethanol, glycerol, n-butanol and methanol): thermodynamic modelling. International Journal of Hydrogen Energy 2011; 36(3):2057–75. URL: http://www.sciencedirect.com/science/article/pii/S0360319910022664.
[30] Yong Z, Mata A, Rodrigues E. Adsorption of carbon dioxide onto hydrotalcite-like compounds (HTLCS) at high temperatures. Industrial & Engineering Chemistry Research 2001;40(1):204–9. URL: http://dx.doi.org/10.1021/ie000238w.
[31] Ficicilar B, Dogu T. Breakthrough analysis for $CO_2$ removal by activated hydrotalcite and soda ash. Catalysis Today 2006; 115(1–4):274–8. URL: http://www.sciencedirect.com/science/article/pii/S0920586106001441.
[32] Rossi C, Cardozo-Filho L, Guirardello R. Gibbs free energy minimization for the calculation of chemical and phase equilibrium using linear programming. Fluid Phase Equilibria 2009;278(1–2):117–28. URL: http://www.sciencedirect.com/science/article/B6TG2-4VGF3TM-1/2/13ad338b07ca73f162b0f742ea99a6f6.
[33] Rabenstein G, Hacker V. Hydrogen for fuel cells from ethanol by steam-reforming, partial-oxidation and combined auto-thermal reforming: a thermodynamic analysis. Journal of Power Sources 2008;185(2):1293–304. URL: http://www.sciencedirect.com/science/article/B6TH1-4T72WVC-6/2/26ff8ad784d4468437891cfaaf9f69f8.
[34] Rossi C, Alonso C, Antunes O, Guirardello R, Cardozo-Filho L. Thermodynamic analysis of steam reforming of ethanol and glycerine for hydrogen production. International Journal of Hydrogen Energy 2009;34(1):323–32. URL: http://www.sciencedirect.com/science/article/B6V3F-4TY8W48-4/2/c7da156e9a6735a6b3f2a5cdd1f371c6.
[35] VanNess HC, Abbott MM. Perry's chemical engineers' handbook. 7th ed. McGraw-Hill Companies, Inc; 1999. Ch. Thermodynamics, pp. 4.1–4.36.
[36] Smith JM, VanNess HC, Abbott MM. Introduction to chemical engineering thermodynamics. 7th ed. New York: McGraw-Hill Companies, Inc.; 1999.
[37] Díaz Alvarado F, Gracia F. Steam reforming of ethanol for hydrogen production: thermodynamic analysis including different carbon deposits representation. Chemical Engineering Journal 2010;165(2):649–57. URL: http://www.sciencedirect.com/science/article/B6TFJ-515SRNK-3/2/018dc5ad079b26a1a563ed60ac46660e.
[38] Liley PE, Thomson GH, Friend DG, Daubert TE, Buck E. Perry's chemical engineers' handbook. 7th ed. McGraw-Hill Companies, Inc.; 1999. Ch. Physical and Chemical Data, pp. 2.1–2.374.
[39] Outokumpu RO. Hsc chemistry 5.1, software. Finland; 2002.
[40] Gozzi D, Iervolino M, Latini A. The thermodynamics of the transformation of graphite to multiwalled carbon nanotubes. Journal of the American Chemical Society 2007;129(33): 10269–75. URL: http://pubs.acs.org/doi/abs/10.1021/ja072120d.
[41] Gaur U, Wunderlich B. Thermodynamic properties of linear macromolecules, part II. polyethylene. Journal of Physical and Chemical Reference Data 1981;10(4):1051.
[42] Wunderlich B, Baur H. Heat capacities of linear high polymers. In: Heat capacities of linear high polymers. Advances in polymer science, vol. 7. Berlin/Heidelberg: Springer. p. 151–368. doi:10.1007/BFb0051029. URL: http://dx.doi.org/10.1007/BFb0051029; 1970.

[43] Moreira RFPM, Soares JL, Casarin GL, Rodrigues AE. Adsorption of $CO_2$ on hydrotalcite-like compounds in a fixed bed. Separation Science and Technology 2006;41(2):341–57. URL: http://www.informaworld.com/10.1080/01496390500496827.

[44] Kuramoto K, Fujimoto S, Morita A, Shibano S, Suzuki Y, Hatano H, et al. Repetitive carbonation-calcination reactions of Ca-based sorbents for efficient $CO_2$ sorption at elevated temperatures and pressures. Industrial & Engineering Chemistry Research 2003;42(5):975–81.

[45] Lu H, Reddy EP, Smirniotis PG. Calcium oxide based sorbents for capture of carbon dioxide at high temperatures. Industrial & Engineering Chemistry Research 2006;45(11):3944–9.

[46] Eaton JW. GNU octave, version 3.2.4. University of Wisconsin, Department of Chemical Engineering. URL: http://www.gnu.org/software/octave/; 2009.

[47] Lucas Rosado PL, Ávarez Ayllón A, Saldaña D, Vega W, Raygoza Garay JA, Noffke P, et al. GNU QToctave, version 0.9.2. URL: http://qtoctave.wordpress.com/; 2010.